JOURNAL OF MATERIALS SCIENCE **41** (2006) 199–210

Kinetics of ferroelectric domains: Application of general approach to $LiNbO_3$ and $LiTaO_3$

VLADIMIR YA. SHUR
Ferroelectric Laboratory IPAM, Ural State University, Ekaterinburg, Russia
E-mail: vladimir.shur@usu.ru

We review the most interesting aspects of the domain structure kinetics in ferroelectrics important for "domain engineering" and discuss them in the framework of a unified nucleation approach. In our approach the nucleation rate is determined by the local value of electric field produced not only by bound charges and voltage applied to the electrodes, but also by screening charges. As a result, any kinetically produced domain pattern, even being far from the equilibrium, can be stabilized by bulk screening. The domain evolution represents a self-organizing process in which the screening of polarization plays the role of feedback. The general approach was applied for the description of the domain kinetics in lithium niobate and lithium tantalate as the most versatile materials for applications. The revealed original scenarios of the domain structure evolution are attributed to the retardation of the screening processes. The decisive role of screening effectiveness for shapes of individual domains and scenarios of the sideways domain wall motion is demonstrated both experimentally and by computer simulation. The possibility to produce a self-assembled nano-scale domain structures with controlled periods has been shown.

1. Introduction

A new branch of science and technology directed to the creation of periodic and quasi-periodic domain structures with desired parameters in commercially available ferroelectrics denoted as "domain engineering" is rapidly developing nowadays. Domain engineering in ferroelectric crystals, such as lithium niobate $LiNbO_3$ (LN) and lithium tantalate $LiTaO_3$ (LT), has revolutionized their use in nonlinear optical applications [1, 2]. The performance of LN and LT as an electro-optic, photorefractive, piezoelectric, and nonlinear optical crystals, make them useful for many different applications. It has been shown that LN and LT with periodical 1*D*- and 2*D*-domain structures possessing an efficient quasi-phase-matching open up a wide range of possibilities for bulk and waveguide nonlinear optical devices [2–4]. During ten years after the first electrical poling of bulk LN samples [5], research on periodically poled LN and LT is under intense interest around the world resulting in production of photonic devices. Breaking the micron-period barrier for periodical domain patterning in LN and LT is very desirable for several new electro-optic applications such as tunable cavity mirrors, which need a periodicity of about 350 nm. The most efficient exploitation of engineered sub-micron domain gratings in LN and LT is related with the waveguide photonic devices.

The switching by application of the external field using the electrode patterns produced by photolithography is the most popular method of periodical poling. Fabrication of the precisely governed regular domain patterns with periods about several microns needs the solution of key problems hindering the improvement of the characteristics of electro-optical and nonlinear optical devices [1]. The broadening of the domains out of electrode area leads to violation of duty-cycle and period due to domain merging. Loss of stability is a great problem for production of sub-micron domain patterns. The uniformity of the domain patterns is destroyed in the bulk. It is impossible to produce the individual domains with desirable shapes which is important for 2*D* patterning. It is clear that the understanding of the physical basis of the domain engineering is the only way to overcome the listed problems. The polarization reversal phenomenon demonstrating essential dependence on the experimental conditions and material still waits for a systematic explanation based on a universal approach.

0022-2461
DOI: 10.1007/s10853-005-6065-7

We present the systematic explanation of the experimental investigations of the domain kinetics in a wide range of domain growth velocities in uniaxial ferroelectrics with optically distinguished domains, LN and LT. We investigate in detail the domain evolution using *in situ* optical observation of the instantaneous domain patterns under application of an electric field. "Slow", "fast" and "super-fast" domain boundary motion regimes have been revealed and investigated. It was claimed that the key property for proposed classification is the screening effectiveness. The crucial role of the intrinsic or artificial dielectric surface layer is clearly exhibited as well. Computer simulation has been used for a verification of the proposed models.

In this paper we introduce the experimental evidence and theoretical considerations which reveal the kinetic nature of the observed domain configurations. In other words, the real domain configurations are determined by the domain kinetics prehistory. We demonstrate the crucial role of the bulk screening processes in the stabilization of the metastable domain structures [6–8]. This approach allows one to choose the proper experimental conditions for stabilization of almost any domain pattern.

2. Domain structure evolution during polarization reversal

Direct experimental visualization of domain kinetics has revealed four main stages of domain evolution [9].

The first stage, "*nucleation of new domains*", develops in perfect crystals at the surface only. The nucleation probability $p \sim \exp(-E_{ac}/E_{loc})$ is determined by activation field E_{ac}, which depends on intrinsic material properties, shape of nuclei and temperature, and electric field averaged over the volume of the nucleus E_{loc}. Experimental observation reveals the nucleation sites at intrinsic or artificial surface defects [8]. The facilitation of the nucleation in real crystals at the given sites is caused by: (1) frozen-in spatial inhomogeneity of E_{ac} due to presence of structural defects, (2) singularities of E_{loc} along the edges of finite electrodes, and (3) E_{loc} created by field concentrators resulting from pits at the sample surface. Moreover it is an open question weather the initial domain state is single-domain or contains the nano-scale residual domains [8, 9]. In the latter case the nucleation of new domains represents a field-induced transition of the "invisible" residual nano-domains into "visible" ones.

The second stage, "*forward growth*", represents an expansion of the formed "nuclei" in polar direction through the sample. All domains at this stage have the charged domain walls and needle-like shape is the most typical. For example, the ratio of the longitudinal to transversal domain sizes in *LN* reaches one hundred [10].

The third stage, "*sideways domain growth*", represents the domain expansion by wall motion in the direction transversal to the polar axis. This stage is the best studied experimentally by *in situ* optical observation of domains. The wall motion anisotropy results in formation of the polygon domains with sides oriented along crystallographic directions.

The fourth stage, "*domain coalescence*", prevails at the completion of the switching process. At this stage the sideways wall motion decelerates. The walls halt and the residual region between walls disappears very rapidly after certain rest time. This process causes the jump-like switching behavior. It is displayed as a noise component of the switching current, known as Barkhausen noise [11–13].

3. General consideration

We discuss all experimentally observed stages of domain kinetics from a unified point of view. According to this approach, the domains with different orientation of spontaneous polarization are considered as the regions of different phases divided by domain walls which represent the phase boundaries. Thus the domain structure evolution during switching is an example of a first-order phase transformation.

The theory of a first-order phase transformation based on kinetic theory of nucleation in its classical version is 80 years old [14, 15]. Nevertheless up to now it is still an active field of research [16].

This approach has been used for description of the growth of solid fraction during crystallization of metals in famous Kolmogorov–Mehl–Johnson–Avrami (KMJA) theory [17, 18]. Ishibashi and Takagi have applied KMJA theory for explanation of the time dependence of the ferroelectric switching current behavior [19].

We will demonstrate how the consistent application of the concepts of the first-order phase transformation theory can be used for explanation of the main features of the domain kinetics during polarization reversal. In this approach all above mentioned stages of the domain kinetics are governed by evolution of thermally activated nuclei with a preferred orientation of the spontaneous polarization.

The nucleation processes: The domain kinetics under application of electric field is governed by competition between nucleation processes of different dimensionalities. Each nucleus represents the minimum domain with preferential orientation of the spontaneous polarization determined by the direction of the local electric field. The appearance of new domains is due to formation of three-dimensional ($3D$) nuclei. The domain growth by motion of the domain walls is a result of $2D$-nucleation (generation of the steps at the wall) and $1D$-nucleation (step growth along the wall). The nucleation probability depends on E_{loc}, being the driving force of all nucleation processes during polarization reversal [8].

Local value of electric field: The internal electric field E_{loc} representing a superposition of electric fields produced by different sources is essentially inhomogeneous. In a ferroelectric capacitor $E_{loc}(r, t)$ is determined mainly by the sum of (1) the external field $E_{ex}(r)$, produced by the voltage applied to the electrodes, (2) the depolarization field $E_{dep}(r, t)$ produced by bound charges developing as a result of spatial inhomogeneity of the spontaneous polarization, (3) the external screening field $E_{scr}(r, t)$ originating from the redistribution of the charges at the electrodes, and (4) the bulk screening field $E_b(r, t)$ governed by bulk screening processes [6–8].

$$E_{loc}(r, t) = E_{ex}(r) + E_{dep}(r, t) + E_{scr}(r, t) + E_b(r, t) \quad (1)$$

The external field $E_{ex}(r)$ strongly depends on the electrode shape. It demonstrates the singularities in the surface layer at the electrode edges due to the fringe effect. This effect is the most pronounced in the vicinity of the ends and corners of the stripe electrodes. The field singularities lead to the dominance of primary nucleation at the electrode boundary. Thus the start of the switching process at the threshold field is determined by field singularities at the electrode edges. It is clear that the "real value" of the threshold field is essentially higher than the value obtained under the common assumption that the switching field is equal to applied potential difference divided by sample thickness.

The depolarization field $E_{dep}(r, t)$ is produced by bound charges existing at the polar surfaces of the sample and at the charged domain walls ("head-to-head" or "tail-to-tail"). For typical ferroelectrics E_{dep} in single-domain plate can reach 10^8–10^9 V/m. This enormous value is essentially reduced for narrow domains and especially for the needle-like ones. That is the reason why triangular and spindle nuclei shapes are the most favorable ones. E_{dep} decelerates the sideways wall motion and limits the wall shift from the initial state. The screening processes diminish the impact of E_{dep}. Thus for low switching rate E_{dep} can be compensated almost totally and complete switching can be observed. For high switching rate the screening retards and applied field leads only to a small wall shift. In this case the initial domain state recovers after switch-off of the external field ("backswitching"). The screening processes can be divided in external and bulk screening.

External screening in ferroelectric capacitor is caused by a current in external circuit. Its rate is defined by the characteristic time of the external circuit τ_{ex}. This time constant is determined by the product of resistance and capacity of the circuit, and usually ranges from nanoseconds to microseconds. The experimentally observed switching time t_s cannot exceed τ_{ex}.

The fast external screening never compensates E_{dep} completely due to existence of the intrinsic dielectric surface layer ("dielectric gap" or "dead layer") [8, 20]. For ferroelectric capacitor of the thickness d the bulk residual depolarization field E_{rd} remains in the area, freshly switched from one single-domain state to another one, even after complete external screening due to existence of the dielectric layer of thickness L and dielectric permittivity ε_L [8, 20]:

$$E_{rd} = E_{dep} - E_{scr} = (2L/d)(P_S/(\varepsilon_L \varepsilon_o)) \quad (2)$$

where P_S is spontaneous polarization.

The existence of the residual depolarization field is the reason why "slow" bulk screening processes are very important.

Bulk screening is the only way to compensate E_{rd}. Three bulk screening mechanisms are considered usually: (1) redistribution of the bulk charges [8, 20], (2) reorientation of the defect dipoles [21], and (3) injection of carriers from the electrode through the dielectric gap [22]. The time constants of all considered mechanisms τ_b range from milliseconds up to months. While E_{rd} is several orders of magnitude less than E_{dep}, nevertheless it is of the same order as experimentally observed threshold fields. For short field pulse the bulk screening of the new state lags behind. Thus such switching is ineffective for irreversible change of the domain structure.

The cooperative action of E_{rd} and E_b leads to the backswitching after switch-off of the external field. This effect could be observed in the areas where $E_{loc}(r, t)$ exceeds the threshold field E_{th}, i.e.

$$\begin{aligned} E_{loc}(r, t) &= -[E_{dep}(r, t) - E_{scr}(r, t) + E_b(r, t)] \\ &= -[E_{rd}(r, t) + E_b(r, t)] > E_{th} \end{aligned} \quad (3)$$

The limiting values of screening effectiveness leads to different variants of domain kinetics after field switch-off: (1) for ineffective bulk screening the initial domain state can be reconstructed completely; (2) for effective bulk screening almost any field-induced domain pattern can be stabilized.

It has been shown experimentally that each of domain kinetics stages can develop according to different scenarios which are strongly dependent on bulk screening effectiveness. The critical values of the applied fields and switching rates corresponding to replacement of domain kinetic scenarios are dependent on material and experimental conditions. The crucial parameter determining the selection of the particular scenario of the domain kinetics is the ratio R between switching rate $(1/t_s)$ and bulk screening rate $(1/\tau_{scr})$. Here t_s is the switching time and τ_{scr} is the screening time constant [23]. Three ranges of the bulk screening effectiveness are considered: (1) $R \ll 1$—"complete screening", (2) $R > 1$—"incomplete screening", and (3) $R \gg 1$ — "ineffective screening". In the following Sections we discuss the domain kinetic scenarios for sideways domain wall motion and growth of

individual domain, which is crucial for manufacturing of engineered 1*D* and 2*D* periodical domain structures.

It must be stressed that static ferroelectric domain structure configuration obtained under application of the proposed approach differs from the equilibrium domain structures obtained in classical theory [11]. The equilibrium multi-domain state is determined in this theory by the minimum of the total free energy. Only two limiting types of the equilibrium domain structures can exist according to this approach. First, the periodical laminar or maze domain structure with neutral domain walls forms if the screening effects are neglected. The domain period is determined by the values of spontaneous polarization, dielectric permittivity, density of the domain wall energy, and sample thickness [9, 11]. Second type demonstrates the absence of any domain structure (single-domain state without domain walls) due to complete screening of the depolarization field. It is well-known that both classical predictions contradict experimentally observed domain patterns. In contrast our approach predicts that practically any domain pattern can be produced and stabilized. These metastable domain structures remain for a long time (about months and years) and present a static one for any application.

It is clear that the domain kinetics depends also on the mechanical properties of the material due to electromechanical coupling. In proper ferroelectrics the first order corrections to the driving force due to piezoelectric effect leads to renormalization of the local value of the switching field [11]. Gopalan *et al*. [24] explained the hexagonal shape of the isolated domains in LN taking into account the anisotropy of the domain wall energy induced by piezoelectric effect. In this paper these effects are accounted for implicitly. We assume that the electromechanical coupling leads to observed anisotropy of the nucleation processes. This fact allows us to explain the experimentally observed continuous transformation of the of domain shape from regular hexagon to three-ray stars (see Section 6).

4. Materials and experimental conditions

The discussed general consideration has been applied for explanation of the domain kinetics in lithium niobate $LiNbO_3$(LN) and lithium tantalate $LiTaO_3$(*LT*). These materials are widely used for creation of periodically poled structures for nonlinear optical applications. The production of the precise tailored periodical domain structures requires the deep understanding of the domain kinetic processes in an inhomogeneous electric field produced by electrode patterns.

LN and LT are the favorite objects of the domain engineering, in spite of the fact that the coercive fields in the most popular congruent compositions (CLN and CLT) are enormously high (about 210 kV/cm). For many years both materials were classified as "frozen ferroelectrics". Quite recently new LN and LT families of crystals closer to stoichiometric composition (SLN and SLT) demonstrating essentially lower coercive fields have become available [25–28].

These crystals are uniaxial with C_3 symmetry in the ferroelectric phase and domain structure with 180° domain walls only. The domain walls are visualized due to pronounced electro-optical effects and direct optical methods can be used for *in situ* observation of the domain kinetics [29, 30]. In the framework of our approach the experimentally observed optical contrast of the domain walls and "domain wall prints" (see Section 5) can be attributed to change of the refractive index induced by incompletely compensated depolarization field in the vicinity of the domain wall [23].

Our switching experiments were held in optical-grade single-domain wafers cut perpendicular to the polar axis and carefully polished. The thickness for CLN and CLT ranges from 0.2 to 0.5 mm, and for SLN and SLT – from 1 to 2 mm.

For the *in situ* investigation of the domain kinetics in an uniform electric field we prepared 1-mm-diameter circular transparent electrodes of: (1) liquid electrolyte (water solution of LiCl) in a special fixture and (2) In_2O_3: Sn (ITO) films deposited by magnetron sputtering. The used electrode sizes allow visualizing the domain kinetics over the whole switched area with enough spatial resolution. The direct observations of the domain evolution were carried out using a polarizing microscope with simultaneous TV-recording and subsequent processing of the image series.

For the periodical poling the wafers were lithographically patterned with periodic stripe metal electrodes deposited on Z^+-surface only and oriented along one of *Y*-directions. The patterned surface was covered by a photoresist layer. High voltage pulses producing an electric field greater than the coercive one were applied through the fixture containing a saturated water solution of LiCl (Fig. 1). The domain patterns produced by partial poling were revealed on both *Z*-surfaces by etching using pure hydrofluoric acid (HF) at room temperature. The obtained surface relief was visualized by optical microscopy, scanning electron microscopy (SEM) and atomic force microscopy (AFM). Moreover we have used the methods of domain visualization without etching by optical microscopy with phase contrast and by piezoelectric force microscopy (PFM) [31].

5. Sideways domain wall motion

5.1. Slow domain growth

"Slow domain growth" is obtained for complete bulk screening ($R \ll 1$). In this case the switching process in

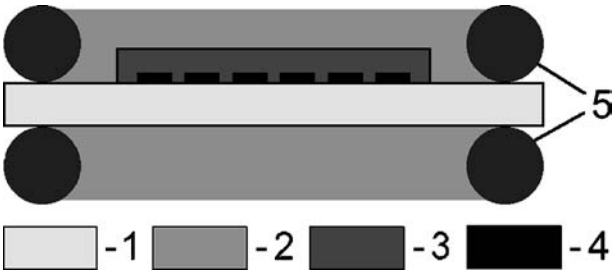

Figure 1 Experimental setup used for periodical poling: 1—wafer, 2—liquid electrolyte, 3—insulating layer, 4—periodic electrodes, 5—O-rings.

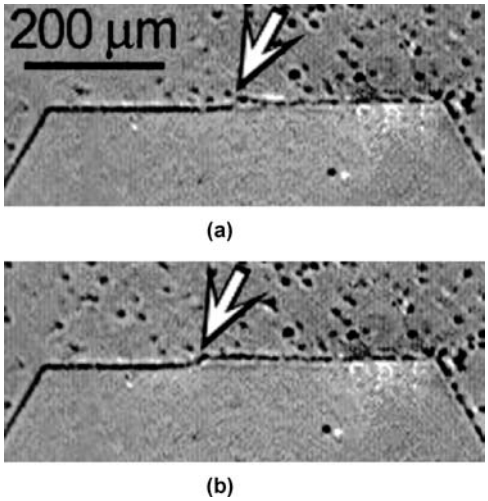

Figure 2 *In situ* optical visualization of the layer-by-layer domain growth by step propagation along the wall in CLN. Time intervals from field switch-on: (a) 1.20 s, (b) 1.28 s. Liquid electrodes. E_{ex}=220 kV/cm.

SLT, CLN and SLN is achieved through the sideways motion of the walls strictly oriented along the *Y*-directions.

In situ observation of the domain kinetics shows that the switching always starts with nucleation at the electrode edges or at the artificially produced surface defects in the center of the electrode area in accordance with our approach [32, 33].

Domain wall motion usually proceeds via the propagation along the wall of an optically distinguished micro-scale domain steps (bunches of the elementary nano-scale steps) (Fig. 2) [32–34], thus confirming above discussed approach. The wall decelerates while shifting from the initial position and partial backswitching is observed after field switch-off.

For quantitative description of the deceleration effect let us consider the shift of the single plane domain wall from the initial state with accomplished bulk screening (E_{rd} completely compensated by the bulk screening). For slow bulk screening the spatial distribution of E_b remains fixed during field-induced wall shift and becomes asymmetric relatively to the shifted wall. In this case E_b is codirectional with E_{rd} in the switched area. The total field at the wall averaged over the sample thickness ΔE_{loc} coincides with the field produced by a stripe capacitor with the width equal to the wall shift Δx and the surface charge determined by the doubled bulk screening charge density $2\sigma_b$ [34–36]

$$\Delta E_{loc}(\Delta x) = (2\sigma_b/\varepsilon\varepsilon_o)F(\Delta x/d) \qquad (4)$$

where $F(\Delta x/d) = 1/\pi[2\text{arctg}(\Delta x/d) + (\Delta x/d)\ 1\text{n}\ (1 + d^2/\Delta x^2)]$, and σ_b=$2P_s(\varepsilon/\varepsilon_L)$L/*d*.

The decelerating field at the wall increases with Δx thus suppressing the step generation (2*D*-nucleation). As a result the wall motion velocity diminishes and the wall stops at some distance from the initial position. After external field switch-off the action of $E_{rd}+E_b$ leads to return of the domain wall to the initial state ("complete backswitching"). The experimentally obtained field dependence of the wall shift measured during step-by-step increase of E_{ex} amplitude is fairly well described by Equation 4 [36].

When the generation of the individual steps is suppressed due to the incomplete screening ($R>1$), two unusual scenarios of sideways wall motion can be realized: (1) loss of the domain wall stability through formation of the finger structure, and (2) acceleration of the wall motion due to domain merging.

5.2. Loss of the domain wall shape stability

The perturbation of the planar wall shape leads to a loss of the domain wall shape stability through formation of the self-assembled domain structure with sub-micron fingers (Fig. 3). The effect is the most pronounced while switching with artificial dielectric layer. The perturbation of the domain wall shape can be induced by (1) inhomogeneity of E_{loc} due to electrode shape irregularity or (2) local decreasing of the threshold field. The perturbation of the domain wall shape evolves forming a ledge ("finger") strictly oriented along *Y*-direction (Fig. 3a). The correlated nucleation, leading to peculiarities of E_{loc} spatial distribution, result in the appearance of the neighboring fingers and propagation of the finger structure along the wall (Fig. 3b). The decelerating effect for shifted wall, characterized by $E_{loc}(\Delta x)$, is suppressed for a finger tip due to diminishing (comparatively with the plane wall) of the neighboring switched area, which is the source of ΔE_{loc} (see Equation 3). Finally the correlated finger structure forms along the wall (Fig. 3c). During periodical domain poling this mechanism provides the abnormal "domain broadening" (large shift of the domain wall from the electrode edge), which is extremely undesirable for periodical poling. The "fingering" leads to the domain merging, thus destroying the periodicity of the domain pattern [37–39].

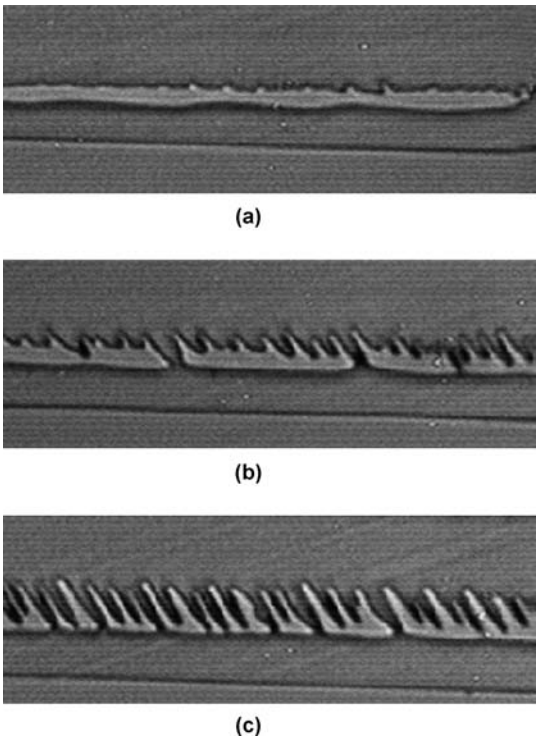

Figure 3 Loss of the wall shape stability during switching in CLN in the area covered by artificial dielectric layer. Stages of the structure evolution. Optical observation of domains revealed by etching.

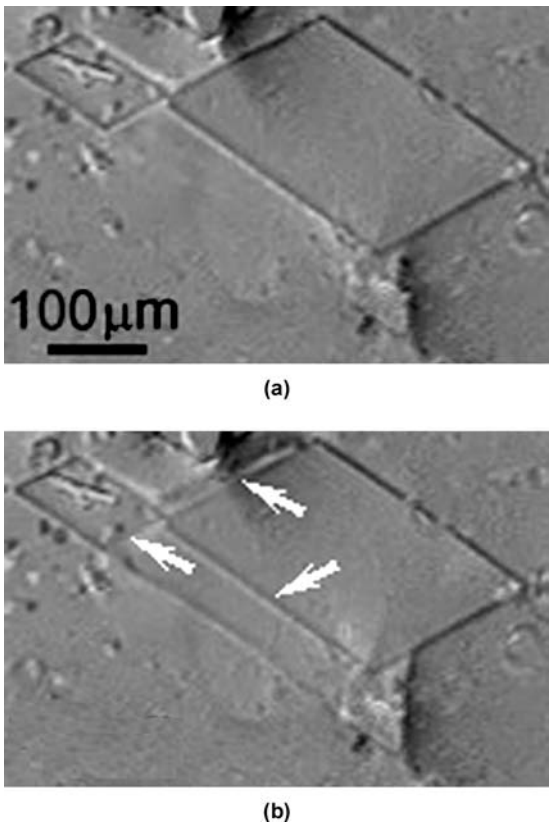

Figure 4 *In situ* optical visualization of "domain gulping" during reversal poling in uniform field in *CLN*. Arrows indicate the domain wall prints. Time interval between the frames 0.04 s. Liquid electrodes. E_{ex}=153 kV/cm.

5.3. Acceleration of the domain wall motion

Although the step generation probability becomes negligible for incomplete screening ($R > 1$), the applied field is strong enough for the step growth. That is the reason why the domain wall propagation can be accelerated by domain merging (Fig. 4), which leads to an effective generation of a great number of steps at the wall. These steps rapidly propagate along existing walls [32–34]. As a result the local deviation of the wall orientation from the allowed crystallographic directions disappears (Fig. 4b). The obtained abnormally fast domain growth ("domain gulping") is followed by easily visualized memory effect caused by retardation of the bulk screening.

"Domain wall prints" remain at the places, where the walls stay for a comparatively long-time before jump to a new position induced by merging (Fig. 4b). Such effect can be understood if we take into consideration the electro-optical nature of the observed contrast of the domain walls. The calculated bulk distribution of E_{loc} in the ferroelectric capacitor with dielectric surface layer demonstrates the field increase in the vicinity of the static domain wall [38]. The field induced variation of the refractive index leads to observed optical contrast of the domain wall. It is clear that E_b also demonstrates a spatial anomaly in the vicinity of the wall (see Equation 1). After the wall jump the domain wall prints fade gradually due to comparatively slow bulk screening process. The print life-time is defined by the bulk screening time constant. This effect has been experimentally observed in CLT by Gopalan and Mitchell [40].

The above discussed acceleration effect prevails for switching from multi-domain initial state with high concentration of small isolated domains. The switching rate for "step generation by merging only" mechanism is determined by only one parameter—the concentration of the individual domains in the initial state. The complete switching can be achieved if the relative concentration exceeds the critical value, which is about 0.02 according to our computer simulations on triangular lattice [41]. The discussed switching scenario prevails for the first switching in CLT [42, 43], which starts with a formation of sub-micron-diameter domains with a density about 1000 mm^{-2} (Fig. 5). It leads to an acceleration of the domain wall motion velocity by more than two orders of magnitude from 1 μm/s for isolated domains to 130 μm/s (for E_{ex}=190 kV/cm).

5.4. Super-fast motion of the switching front

In strong enough fields the switching process can continue even for absolutely ineffective bulk screening ($R \gg 1$). In this case the continuous motion of the wall is absolutely

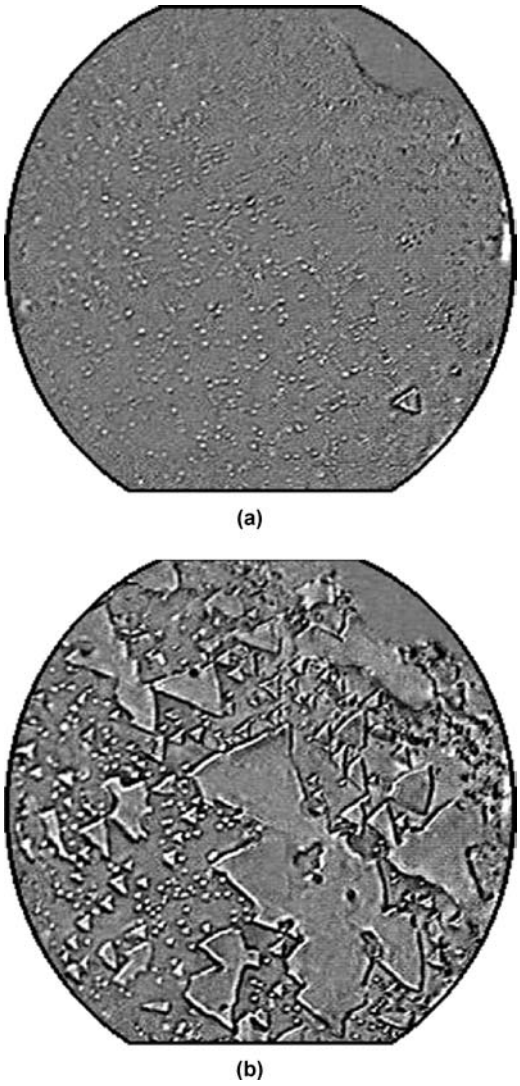

Figure 5 *In situ* optical visualization of the domain kinetics during switching in *CLT*. Time intervals from the field switch-on: (a) 0.3 s, (b) 0.9 s. 1-mm-diameter liquid electrodes. E_{ex}=190 kV/cm.

forbidden and domain growth is achieved through propagation of the boundary of ensemble of isolated needle-like domains. Such "discrete switching" results in super-fast motion of the switching front demonstrating pronounce self-assembling behavior.

This effect has been observed during spontaneous backswitching after abrupt removing of the external switching field in LN and LT crystals with an artificial dielectric surface layer [44–46]. Various self-organized nano-scale domain structures develop (1) arrays strictly oriented along crystallographic directions (Fig. 6a) and (2) stripes (Fig. 6b). Similar effect has been observed during "super-fast switching" in PGO [47, 48].

Formation of all obtained self-assembled structures can be considered as manifestation of the correlated nucleation effect in the vicinity of the shifted domain wall which is stopped by incomplete screening. The correlated

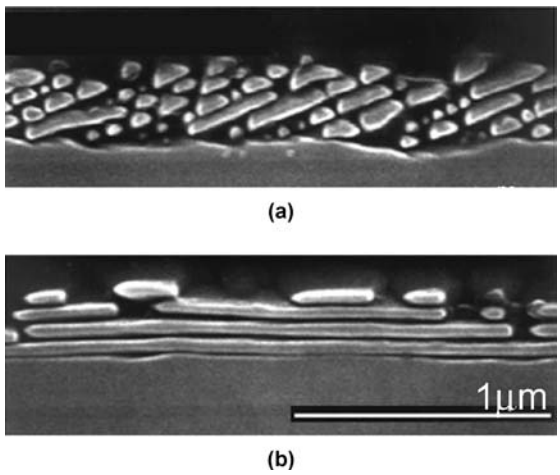

Figure 6 Quasi-periodic nano-scale domain structures: (a) arrays and (b) stripes. Backswitching near the edge of the stripe electrode under the artificial dielectric layer in CLN. SEM images. Domains revealed by etching.

nucleation is caused by a pronounced maximum of E_{loc}, existing in this case in front of the wall at the distance nearly equal to the thickness of the surface dielectric layer L, shown by computer simulation [38]. This field maximum essentially increases the $3D$-nucleation probability in front of the wall thus leading to appearance of isolated domains at the distance L along the boundary. Any arising isolated domain cannot spread out due to suppression of $2D$-nucleation at its wall by the uncompensated E_{dep}. The arising domains repel each other due to electrostatic and electro-mechanical interaction. As a result the quasi-regular domain chain consisting of needle-like domains with submicro- or nano-scale transversal sizes aligns along the wall (Fig. 7). It has been shown by simulation that the new field maximum appears at approximately same distance from the formed domain chain thus initiating formation of the second one [38]. Thus, self-maintained enlarging quasi-regular domain structure can cover the areas of about square millimeters.

The role of the correlated nucleation can be intensified by: (1) increasing of R through rising of the switching field or by hindering of the screening processes, (2) deposition of the artificial surface dielectric layer, thus increasing E_{rd}. The later allows us to control the period of the quasi-regular structure, which is important for domain engineering. It has been revealed experimentally that the velocity of such process exceeds by orders of magnitude the usual wall motion velocity. That is the reason why the process can be named as "super-fast domain growth."

Correlated nucleation plays the most important role during backswitching in CLN after an abrupt removing of the external field. The record value of P_s in LN leads to abnormally high value of E_{rd}, which induces backswitching. The backward motion of the domain wall is achieved through propagation of the highly organized quasi-periodical structure of domain arrays strictly ori-

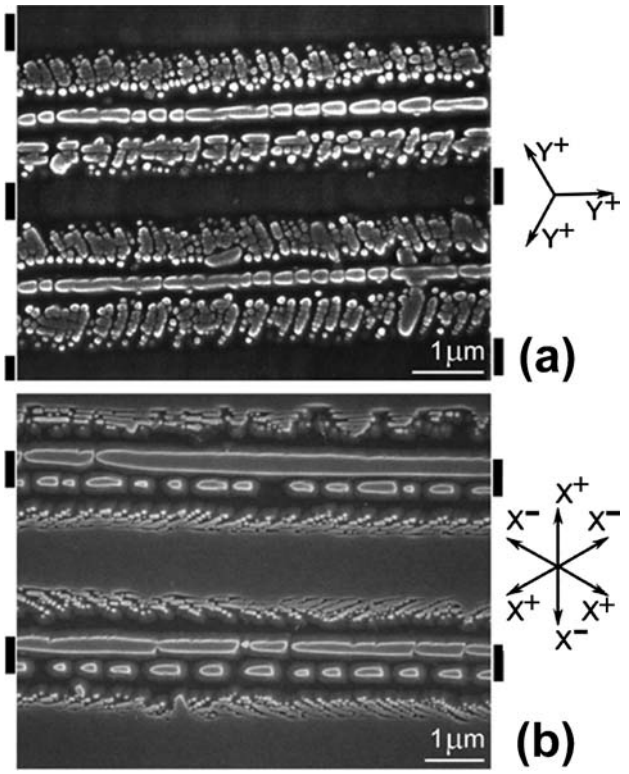

Figure 7 Nanodomain arrays oriented along (a) Y^+ and (b) X-directions. Backswitching near the edge of the stripe electrode under the artificial dielectric layer in CLN. SEM images. Domains revealed by etching. Black rectangles show electrode positions [33].

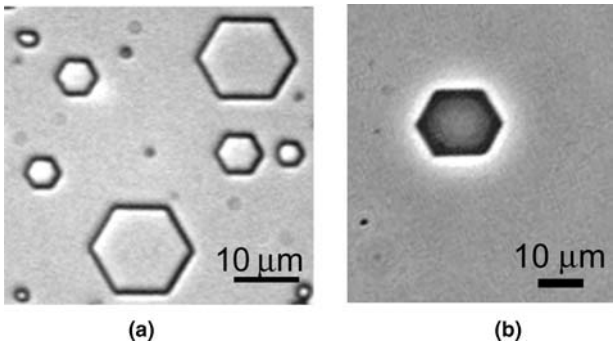

Figure 8 Hexagon domains: (a) CLN, (b) SLT. Optical images: (a) domains revealed by etching, (b) phase-contrast-microscopy [21].

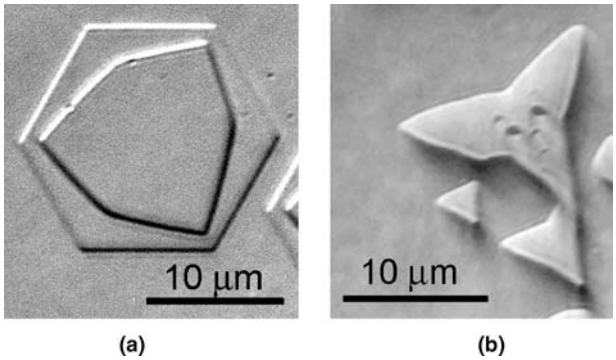

Figure 9 Exotic polygon domains formed during switching in CLN under artificial dielectric layer: (a) convex hexagons, (b) hexagon with concave angles ("Mercedes star") and regular triangle. Domains revealed by etching. (a) Switching by two pulses and etching of Z^- surface after each pulse [21].

ented along crystallographic directions (Fig. 7) [38, 44–46, 49]. Each quasi-regular array is comprised of nano-domains with a diameter 30–100 nm and an average linear density exceeding 10^4 mm^{-1}. Two variants of array orientation are obtained: (1) along the Y^+-direction at 60° to the electrode edges (Fig. 7a) and (2) along the X-directions (Fig. 7b). In the later case the fast growth of nano-domains along electrodes can lead to the formation of a periodic set of nano-scale stripe domains with period about 100 nm (Fig. 6b).

6. Growth of isolated domains

It has been shown experimentally for several ferroelectrics that the shapes of isolated domains growing in uniform electric field essentially depend on the field value [42, 50–53].

6.1. Hexagonal domain shape

The perfect hexagon domains with sides strictly oriented along Y-directions are formed for switching under complete screening ($R<1$) in any LN (Fig. 8a) and SLT (Fig. 8b).

For incomplete screening ($R>1$) E_{rd} suppresses the step propagation along the walls, thus leading to the essential deviation from the hexagonal shape. The domain shapes essentially deviating from the equiangular hexagons forms in LN during very fast switching. Similar effect is observed also in the samples covered by an artificial dielectric layer (Fig. 9).

6.2. Triangular domain shape

Individual domains of triangular shape with the sides strictly oriented along the X-directions were observed in CLN and CLT (Fig. 10). In CLT, the regular triangular domains were always obtained for any switching conditions (Fig. 10a), whereas in CLN such domains form for switching with an artificial dielectric layer or as a result of fast spontaneous backswitching (Fig. 10b).

The observed quantitative difference between domain shapes in CLT (triangles) and SLT or any LN (hexagons) for switching in ordinary conditions can be attributed to the large difference of the screening times. It has been shown experimentally that the screening process in CLT is essentially slower ($\tau_{scr} \sim 1$ s) as compared with LN and SLT ($\tau_{scr} \sim 50$–100 ms). The continuous transformation from hexagons to triangles in CLN induced by incomplete screening is a clear demonstration that the domain shape

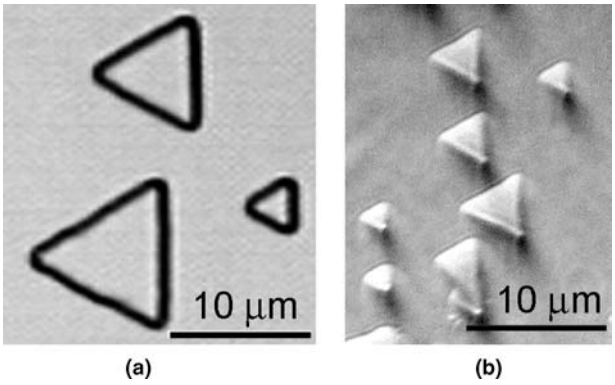

Figure 10 Triangle domains: (a) CLT, (b) CLN (formed during switching under artificial dielectric layer). Optical images. Etch-revealed domains [21].

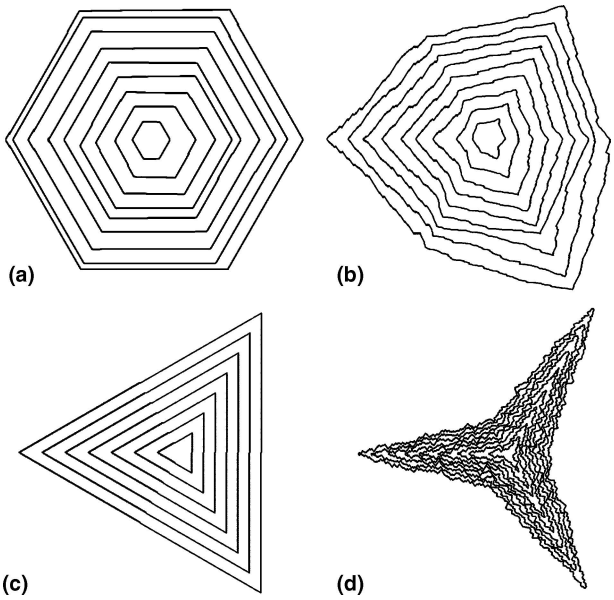

Figure 11 Computer simulation of isolated domain growth. The ratio between the rates of step generation and step growth increases from (a) to (d) [21].

is governed by competition between step generation and step kinetics of domain growth.

We have verified by computer simulation the kinetic nature of the domain shape. The model is based on the experimentally observed main features of the domain growth in crystals with C_3 symmetry. First, the generation of new steps occurs at three vertices of the regular hexagonal isolated domain (Y^+-crystallographic directions). Second, the steps grow along Y^+-directions. The wall orientation is determined by the step concentration similar to formation of vicinal faces during crystal growth. The hexagons are formed for high step growth velocity and low step generation rate (low step concentration) (Fig. 11a).

The variation of the ratios between the step generation and step growth rates due to retardation of the bulk screening changes the domain shape. Existence of a trail

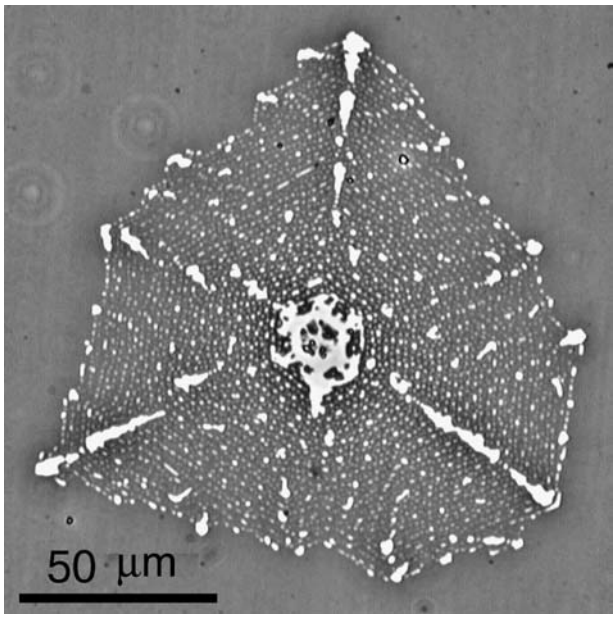

Figure 12 Web-type domain structure for switching with artificial dielectric layer in *SLT*. Optical image. Domains revealed by etching [31].

of uncompensated field following the moving step decelerates the step growth thus increasing the step concentration at the wall. The simulation of the isolated domain growth predicts existence of hexagons, triangles and even polygons with concave angles similar to "Mercedes star" (Fig. 11d). All shapes have been experimentally observed during switching in *CLN* covered by artificial dielectric layer (Fig. 9).

6.3. Web-like domain shape

It is interesting that the similar laws of the domain growth can be observed even during above discussed discrete switching for completely ineffective screening ($R \gg 1$). The effect has been studied during switching in *SLT* completely covered by artificial dielectric layer (photoresist). The switching starts with the formation of a conventional hexagon domain around the pin-hole in the dielectric layer. The subsequent growth is achieved through spreading of the quasi-regular ensemble of micro-scale isolated domains following the same mechanisms as the continuous growth of the isolated domain. The shape of the switched area is the same regular polygon as in the case of growth of isolated domains. The "steps" forms and propagates along the boundary of the ensemble playing the role of the domain wall (Fig. 12). The averaged distance between the nuclei is very close to the thickness of the artificial dielectric gap.

7. Domain engineering

The understanding of the field induced domain kinetics in LN and LT allows us to propose recently an original pol-

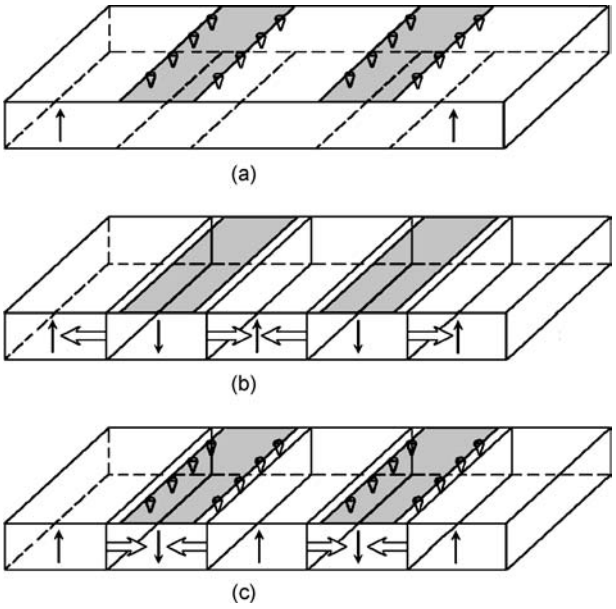

Figure 13 Main stages of the domain evolution during backswitched poling. (a) nucleation, (b) broadening, (c) backswitching after field switch off. White arrows show the directions of the domain wall motion [33].

ing method for creation of short-pitch periodical domain structures, so-called "backswitched poling" [44, 45, 54].

We exploit the unique abilities of the backswitching process, which was always considered as undesirable one, because it destroys the tailored structure. During backswitched poling, several distinguishable stages of domain evolution can be revealed (Fig. 13). The process starts with formation of new domains at the z^+- polar surface along the electrode edges due to the field singularities caused by the fringe effect (Fig. 13a). During the second stage, the domains grow and propagate through the wafer forming the laminar domains. The always observed domain broadening out of the electrode area leads to an essential difference between the lithographically defined electrode pattern and the produced periodical domain structure (Fig. 13b). For short periods domain broadening results in domain merging, thus limiting the production of the short-pitch domain patterns. After rapid decreasing of the poling field, the backswitching starts through shrinkage of the laminar domains by the backward wall motion and formation of the domains with the initial orientation of P_s along the electrode edges (Fig. 13c).

The application of this improved poling method to LN demonstrates the spatial frequency multiplication of the domain patterns as compared to the spatial frequency of the electrodes and self-maintained formation of the oriented domain arrays consisting of individual nano-scale domains [44, 46]. The mechanism of frequency multiplication is based on domain formation along the electrode edges during backswitching. For "frequency tripling" (Fig. 14c), the subsequent growth and merging of the domains lead to formation of a couple of strictly oriented sub-micron-width domain stripes with depth about 20–50 μm under the edges of wide electrodes (Fig. 14d). For narrow electrodes only the "frequency doubling" can be obtained with the depth of the backswitched domain stripes about 50–100 μm (Fig. 14a). The cross sections of the backswitched domain reveal two distinct variants of domain evolution: "erasing" and "splitting". During "erasing" the backswitched domains are formed in the earlier switched area without any disturbance of the external shape of the laminar domain (Fig. 14e). During

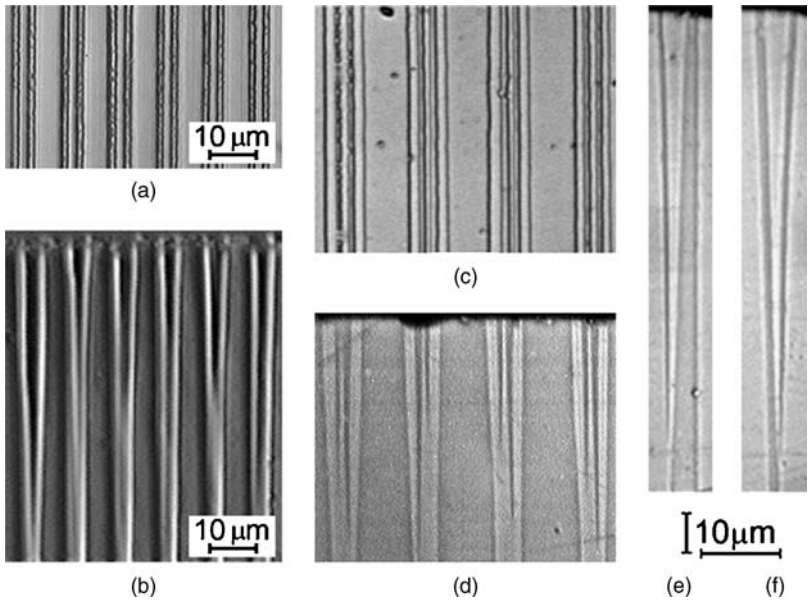

Figure 14 Domain frequency multiplication (a), (b) "doubling," (c), (d) "tripling," (e) "erasing," (f) "splitting". (a), (c) z^+ view, (b), (d), (e), (f) y cross-sections. Optical images. Domains revealed by etching. CLN [33].

"splitting" the backswitched domains cut the switched one conserving its volume and varying the shape (Fig. 14f).

Backswitched poling in *CLN* enables higher fidelity and shorter period domain patterning of thick substrates than can be achieved with conventional poling. 4 μm-period 5-cm-length devices were characterized for continuous-wave (cw) single-pass second harmonic generation (*SHG*) of blue light [45]. First-order single-pass cw *SHG* at 460–465 nm produced 61 mW of power at 6.1%/W efficiency from a Ti:sapphire laser source and 60 mW at 2.8%/W efficiency for a laser-diode source was achieved [55].

8. Conclusion

In the present paper, we have formulated the unified approach to the domain kinetics based on the nucleation mechanism of the polarization reversal and demonstrated its validity for understanding the variety of experimentally observed domain evolution scenarios. We prove that the kinetics of the ferroelectric domain structure essentially depends upon effectiveness of the screening processes. Original scenarios of the domain structure evolution were revealed experimentally and discussed within unified approach accounting for the decisive role of the retardation of the screening process. We demonstrate that the evolution of a domain structure in ferroelectrics during decay of the highly-nonequilibrium state presents the self-organizing process, in which the screening of polarization reversal plays the role of feedback. The discussed results of the fundamental investigations can be used as a physical basis of "domain engineering". We have proposed and realized several new techniques, which allow to produce the short-pitch regular domain patterns with record periods and nano-scale quasi-regular domain structures in lithium niobate and lithium tantalate single crystals. The crystals possessing such regular structures demonstrate new non-linear optical properties required for modern coherent light frequency conversion devices.

Acknowledgements

This work was supported in part by INTAS (Grant 03-51-6562), by RFBR-DFG (Grant 04-02-04007), by RFBR-NNSF (Grant 03-02-39004), by Program "Development of the Scientific Potential of High Education" of Federal Agency of Education (Grant 48859), by Program BRHE of U.S. CRDF and Federal Agency of Education (Award No.EK-005-X1). It is a pleasure to acknowledge the many helpful stimulating discussions with A. Alexandrovski, L.E. Cross, M.M. Fejer, K. Kitamura, A.L. Korzhenevskii, E.L. Rumyantsev, and J.F. Scott.

References

1. R. L. BYER, *J. Nonlinear Opt. Phys. & Mater.* **6** (1997) 549.
2. L. E. MYERS, R. C. ECKHARDT, M. M. FEJER, R. L. BYER, W. R. BOSENBERG and J. W. PIERCE, *J. Opt. Soc. Am. B* **12** (1995) 2102.
3. G. W. ROSS, M. POLLNAU, P. G. R. SMITH, W. A. CLARKSON, P. E. BRITTON and D. C. HANNA, *Opt. Lett.* **23** (1998) 171.
4. N. G. R. BRODERICK, G. W. ROSS, H. L. OFFERHAUS, D. J. RICHARDSON and D. C. HANNA, *Phys. Rev. Lett.* **84** (2000) 4345.
5. M. YAMADA, N. NADA, M. SAITOH and K. WATANABE, *Appl. Phys. Lett.* **62** (1993) 435.
6. V. YA. SHUR and E. L. RUMYANTSEV, *Ferroelectrics* **191** (1997) 319.
7. V. YA SHUR, *Phase Transitions* **65** (1998) 49.
8. V. YA. SHUR, in Ferroelectric Thin Films: Synthesis and Basic Properties, edited by C. A. Paz de Araujo, J. F. Scott and G. W. Taylor (Gordon and Breach, New York, 1996) p. 153.
9. E. FATUZZO and W. J. MERZ, "Ferroelectricity" (North-Holland Publishing Company, Amsterdam, 1967).
10. V. YA. SHUR, E. L. RUMYANTSEV, E. V. NIKOLAEVA, E. I. SHISHKIN, R. G. BATCHKO, G. D. MILLER, M. M. FEJER and R. L. BYER, *Ferroelectrics* **236** (2000) 129.
11. M. E. LINES and A. M. GLASS, "Principles and Application of Ferroelectrics and Related Materials" (Clarendon Press, Oxford, 1977).
12. R. C. MILLER, *J. Phys. Chem. Solids* **17** (1960) 93.
13. V. YA. SHUR, E. L. RUMYANTSEV, D. V. PELEGOV, V. L. KOZHEVNIKOV, E. V. NIKOLAEVA, E. I. SHISHKIN, A. P. CHERNYKH and R. K. IVANOV, *Ferroelectrics* **267** (2002) 347.
14. M. VOLMER, "Kinetik der Phasenbildung" (Steinkopff, Dresden-Leipzig, 1939).
15. YA. B. ZELDOVICH, *Zh. Eksp. Theor. Fiz.* **12** (1942) 525 (in Russian).
16. J. W. P. Schmelzer (ed.) Nucleation Theory and Applications, (Wiley-VCH, Weinheim, 2005).
17. A. N. KOLMOGOROV, *Izv. Acad. Nauk USSR., Ser. Math.* **3** (1937) 355 (in Russian).
18. M. AVRAMI, *J. Chem. Phys.* **7** (1939) 1103.
19. Y. ISHIBASHI and Y. TAKAGI, *J. Phys. Soc. Jap.* **31** (1971) 506.
20. V. M. FRIDKIN, "Ferroelectrics Semiconductors" (Consult. Bureau, New York and London, 1980).
21. P. V. LAMBECK and G. H. JONKER, *J. Phys. Chem. Solids* **47** (1986) 453.
22. A. K. TAGANTSEV, I. STOLICHNOV, E. L. COLLA and N. SETTER, *J. Appl. Phys.* **90** (2001) 1387.
23. V. YA. SHUR, in Nucleation Theory and Applications, edited by J. W. P. Schmelzer (Wiley-VCH, Weinheim, 2005) p. 178.
24. Y. FURUKAWA, K. KITAMURA, S. TAKEKAWA, K. NIWA and H. HATANO, *Opt. Lett.* **23** (1998) 1892.
25. V. GOPALAN, N. A. SANFORD, J. A. AUST, K. KITAMURA and Y. FURUKAWA, in Handbook of Advanced Electronic and Photonic Materials and Devices, edited by H. S. Nalwa (Academic Press, 2001) Ch. 2, p. 57.
26. K. KITAMURA, Y. FURUKAWA, K. NIWA, V. GOPALAN and T. MITCHELL, *Appl. Phys. Lett.* **73** (1998) 3073.
27. K. NIWA, Y. FURUKAWA, S. TAKEKAWA and K. KITAMURA, *J. Crystal Growth* **208** (2000) 493.
28. L. HUANG, D. HUI, D. J. BAMFORD, S. J. FIELD, I. MNUSHKINA, L. E. MYERS and J. V. KAYSER, *Appl. Phys. B* **72** (2001) 301.
29. V. GOPALAN, Q. JIA and T. MITCHELL, *Appl. Phys. Lett.* **75** (1999) 2482.
30. M. MULLER, E. SOERGEL and K. BUSE, *Opt. Lett.* **28** (2003) 2515.
31. A. GRUVERMAN, O. KOLOSOV, J. HATANO, K. TAKAHASHI and H. TOKUMOTO, *J. Vac. Sci. Technol. B* **13** (1995) 1095.
32. V. YA. SHUR, E. L. RUMYANTSEV, E. V. NIKOLAEVA, E. I. SHISHKIN, R. G. BATCHKO, M. M. FEJER, R. L.

BYER and I. MNUSHKINA, *Ferroelectrics* **269** (2002) 189.
33. V. YA. SHUR, E. L. RUMYANTSEV, E. V. NIKOLAEVA, E. I. SHISHKIN, R. G. BATCHKO, M. M. FEJER and R. L. BYER, *ibid.* **257** (2001) 191.
34. M. E. DROUGARD and R. LANDAUER, *J. Appl. Phys.* **30** (1959) 1663.
35. V. YA. SHUR, A. L. GRUVERMAN, V. V. LETUCHEV, E. L. RUMYANTSEV and A. L. SUBBOTIN, *Ferroelectrics* **98** (1989) 29.
36. V. YA. SHUR, E. L. RUMYANTSEV, V. P. KUMINOV, A. L. SUBBOTIN and E.V. NIKOLAEVA, *Phys. Solid State* **41** (1999) 112.
37. G. ROSENMAN, A. SKLIAR and A. ARIE, *Ferroelectrics Review* **1** (1999) 263.
38. V. YA. SHUR, E. L. RUMYANTSEV, E. V. NIKOLAEVA, E. I. SHISHKIN, R. G. BATCHKO, G. D. MILLER, M. M. FEJER and R. L. BYER, *SPIE Proceedings on Smart Structures and Materials* **3992** (2000) 143.
39. V. SHUR, E. RUMYANTSEV, R. BATCHKO, G. MILLER, M. FEJER and R. BYER, *Ferroelectrics* **221** (1999) 157.
40. V. GOPALAN and T. MITCHELL, *J. Appl. Phys.* **85** (1999) 2304.
41. A. P. CHERNYKH, V. YA. SHUR, E. V. NIKOLAEVA, E. I. SHISHKIN, A. G. SHUR, K. TERABE, S. KURIMURA, K. KITAMURA and K. GALLO, *Material Science & Engineering B* **120** (2005) 109.
42. V. YA. SHUR, E. V. NIKOLAEVA, E. I. SHISHKIN, A. P. CHERNYKH, K. TERABE, K. KITAMURA, H. ITO and K. NAKAMURA, *Ferroelectrics* **269** (2002) 195.
43. V. YA. SHUR, E. V. NIKOLAEVA, E. I. SHISHKIN, V. L. KOZHEVNIKOV, A. P. CHERNYKH, K. TERABE and K. KITAMURA, *Appl. Phys. Lett.* **79** (2001) 3146.
44. V. YA. SHUR, E. L. RUMYANTSEV, E. V. NIKOLAEVA, E. I. SHISHKIN, D. V. FURSOV, R. G. BATCHKO, L. A. EYRES, M. M. FEJER and R. L. BYER, *ibid.* **76** (2000) 143.
45. R. G. BATCHKO, V. Y. SHUR, M. M. FEJER and R. L. BYER, *ibid.* **75** (1999) 1673.
46. V. YA. SHUR, E. L. RUMYANTSEV, E. V. NIKOLAEVA, E. I. SHISHKIN, D. V. FURSOV, R. G. BATCHKO, L. A. EYRES, M. M. FEJER, R. L. BYER and J. SINDEL, *Ferroelectrics* **253** (2001) 105.
47. V. YA. SHUR, A. L. GRUVERMAN, N. YU. PONOMAREV, and N. A. TONKACHYOVA, *ibid.* **126** (1992) 371.
48. V. YA. SHUR, A. L. GRUVERMAN, N. YU. PONOMAREV, E. L. RUMYANTSEV and N. A. TONKACHYOVA, *Integrated Ferroelectrics* **2** (1992) 51.
49. V. YA. SHUR, E. V. NIKOLAEVA and E. I. SHISHKIN, *Physics of Low-Dimensional Structures* **3/4** (2003) 139.
50. R. C. MILLER and A. SAVAGE, *Phys. Rev.* **115** (1959) 1176.
51. J. HATANO, F. SUDA and H. FUTAMA, *J. Phys. Soc. Jap.* **45** (1978) 244.
52. V. YA. SHUR, V. V. LETUCHEV and E. L. RUMYANTSEV, *Sov. Phys. Solid State* **26** (1984) 1521.
53. V. YA. SHUR, V. V. LETUCHEV, E. L. RUMYANTSEV and I. V. OVECHKINA, *ibid.* **27** (1985) 959.
54. R. BATCHKO, G. MILLER, R. BYER, V. SHUR and M. FEJER, *United States Patent* No. 6, 542,285 B1, April 1, 2003.
55. R. G. BATCHKO, M. M. FEJER, R. L. BYER, D. WOLL, R. WALLENSTEIN, V. YA. SHUR and L. ERMAN, *Optics Letters* **24/18** (1999) 1293.